frontiers | Frontiers in Earth Science

TYPE Original Research
PUBLISHED 24 May 2024
DOI 10.3389/feart.2024.1399836

OPEN ACCESS

EDITED BY
Hossein Azizi,
University of Kurdistan, Iran

REVIEWED BY
Abdolnaser Fazlnia,
Urmia University, Iran
Fatemeh Nouri,
University of Kurdistan, Iran

*CORRESPONDENCE
Xiaolong Wang,
xiaolong.wang@soremi.net
Wengao Zhang,
547027367@qq.com

RECEIVED 12 March 2024
ACCEPTED 29 April 2024
PUBLISHED 24 May 2024

CITATION
Wang X, Zhang W, Cheng S, Wang B, Tang Y and Li W (2024), Geological characteristics of early cretaceous volcanic rocks and analysis of metallogenic potential of uranium mineralization in Moganshan basin, northern Zhejiang province, China.
Front. Earth Sci. 12:1399836.
doi: 10.3389/feart.2024.1399836

Geological characteristics of early cretaceous volcanic rocks and analysis of metallogenic potential of uranium mineralization in Moganshan basin, northern Zhejiang province, China

Xiaolong Wang[1,2]*, Wengao Zhang[3,4]*, Shenghong Cheng[2], Bo Wang[5], Yifei Tang[6] and Wei Li[1]

[1]School of Earth Science and Resources, Chang'an University, Xi'an, China, [2]SOREMI SA, Point Noire, Republic of Congo, [3]SinoProbe Laboratory, Institute of Geomechanics, Chinese Academy of Geological Science, Beijing, China, [4]Key Laboratory of Paleomagnetism and Tectonic Reconstruction of Ministry of Natural Resources, Institute of Geomechanics, Chinese Academy of Geological Sciences, Beijing, China, [5]Institute of Nuclear Industry, Guanghan, Sichuan, China, [6]Institute of Geologic Survey, China University of Geosciences, Wuhan, China

The Moganshan Volcanic Basin is located in the northeastern section of the Ganhang volcanic-tectonic-uranium polymetallic metallogenic belt. To explore the uranium mineralization potential of these volcanic rocks, petrographic, elemental geochemical, zircon U-Pb chronology, and Sr-Nd-Pb isotope analyses were performed on the volcanic rocks in the Moganshan Basin. The results showed that the volcanic rocks within the Moganshan Basin were formed at 130.8 ± 2.0 Ma; In addition, they are Si-rich (SiO_2 content of 72.98%–77.32%), alkali-rich (Na_2O+ K_2O, with ALK values of =7.15–9.74), and potassium-rich (K_2O/Na_2O content of 1.41–4.34), with light rare earth elements (Rb, Th Nd, Zr, and Hf). Further more, the volcanic rocks within the Moganshan Basin are deficient in Ba, Ta, Nb, and Sr, with a negative europium anomaly (δEu of 0.10–0.17), high ISr (0.71028–0.71160), low εNd(t) values (–6.43–5.77), and other characteristics. The geological characteristics of the volcanic rocks in the Moganshan Basin are the same as those of the volcanic rocks in eastern China, and the formation age is Early Cretaceous. The formation environment is intra-land extensional and tensional. The rock-forming material primarily originates from the upper crust and has a higher average uranium content than that in the Ganhang volcanic belt. Additionally, it is speculated that the Moganshan Volcanic Basin has good potential for uranium mineralization.

KEYWORDS

volcanic rock, early cretaceous, geochemical characteristics, uranium metallogenic potential, Moganshan basin

1 Introduction

The Moganshan Volcanic Basin is located in the northeastern part of the Ganhang volcanic-tectonic-uranium polymetallic metallogenic belt, and there are a series of uranium mineralization anomalies in the basin, most of which are of volcanic type. During more than half a century of research, many studies have been conducted on volcanic uranium ores in the Moganshan Basin in detail in terms of deposit geological characteristics, mineralogy, mineralizing fluids, chronology, and petrography (Wang K. X. et al., 2013; Han et al., 2014; Liu et al., 2018a; Liu et al., 2018b). However, there are still many controversies concerning the genesis of this volcanic rocks and the resource of uranium ore. Most researchers agree that the volcanic rocks in northern Zhejiang is S-type magma which originated from the remelting of the Earth's crust (Dou et al., 2005; Yang et al., 2010; 2012; Ma and Xue, 2017). While others believe that although they have the characteristics of crustal origin, mantle material was added during the formation process, and the mantle material was important for the formation of magma and ore-forming material (Li, 1993; Duan et al., 2001; Fan et al., 2001).

Previous research on the volcanic rocks within the Moganshan Basin has yielded contentious findings regarding their lithological characteristics and petrogenesis. The absence of isotopic geochemical data has hindered a thorough analysis of the magmatic evolution process, thereby limiting the exploration of uranium mineralization potential and the search for uranium deposit. Studies indicate that hydrothermal uranium ore is not lithologically selective but is intimately associated with magmatic rocks from specific periods. Notably, hydrothermal uranium ore linked to volcanic rocks predominantly occurs in the Early Cretaceous high-potassium-calcium-alkaline rhyolite (Wu et al., 2017). Consequently, this study focuses on the Early Cretaceous volcanic rocks of the Moganshan Volcanic Basin. Through comprehensive field geological, petrographic, isotopic chronological, and geochemical investigations, we have systematically elucidated the fundamental geological characteristics of these rocks and delved into their petrogenetic types, diagenetic ages, material sources, and tectonic settings. These insights have facilitated an analysis of the uranium mineralization potential within the Moganshan Volcanic Basin.

2 Geological background

The Ganhang Volcanic-Tectonic Belt, located at the juncture of the Yangtze and Cathaysia plates (Figure 1A), is acknowledged as China's most extensive volcanic uranium mineralization belt. This belt comprises numerous uranium ore fields, such as Xiangshan, Dazhou, and Xinlu, in addition to various concentrated uranium mineralization zones, including Yuhuashan and Gonggong Mountain. The principal ore-bearing rocks, closely linked with uranium mineralization, are the volcanic rocks dating from the Early Cretaceous period (Ma and Xue et al., 2017; Liu et al., 2018b). The Moganshan Basin is located on the northeast side of the Ganhang volcanic belt, and the Early Cretaceous volcanic rocks are widely distributed in the basin, giving the area a large potential for uranium ore search. The main exposed strata in the area are the Silurian, a small amount of Devonian-Carboniferous,

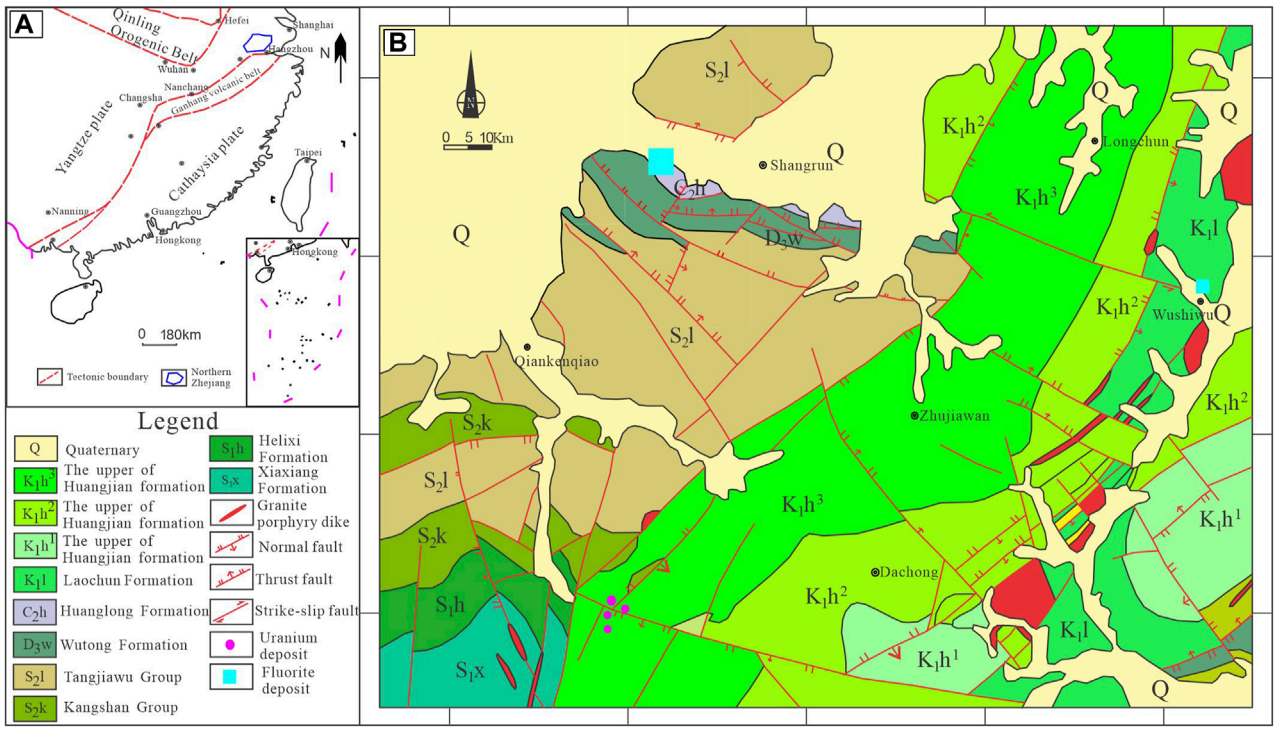

FIGURE 1
Geotectonic position **(A)** and its regional geological sketch **(B)** in northern Zhejiang Province (Wang et al., 2022).

10.3389/feart.2024.1399836

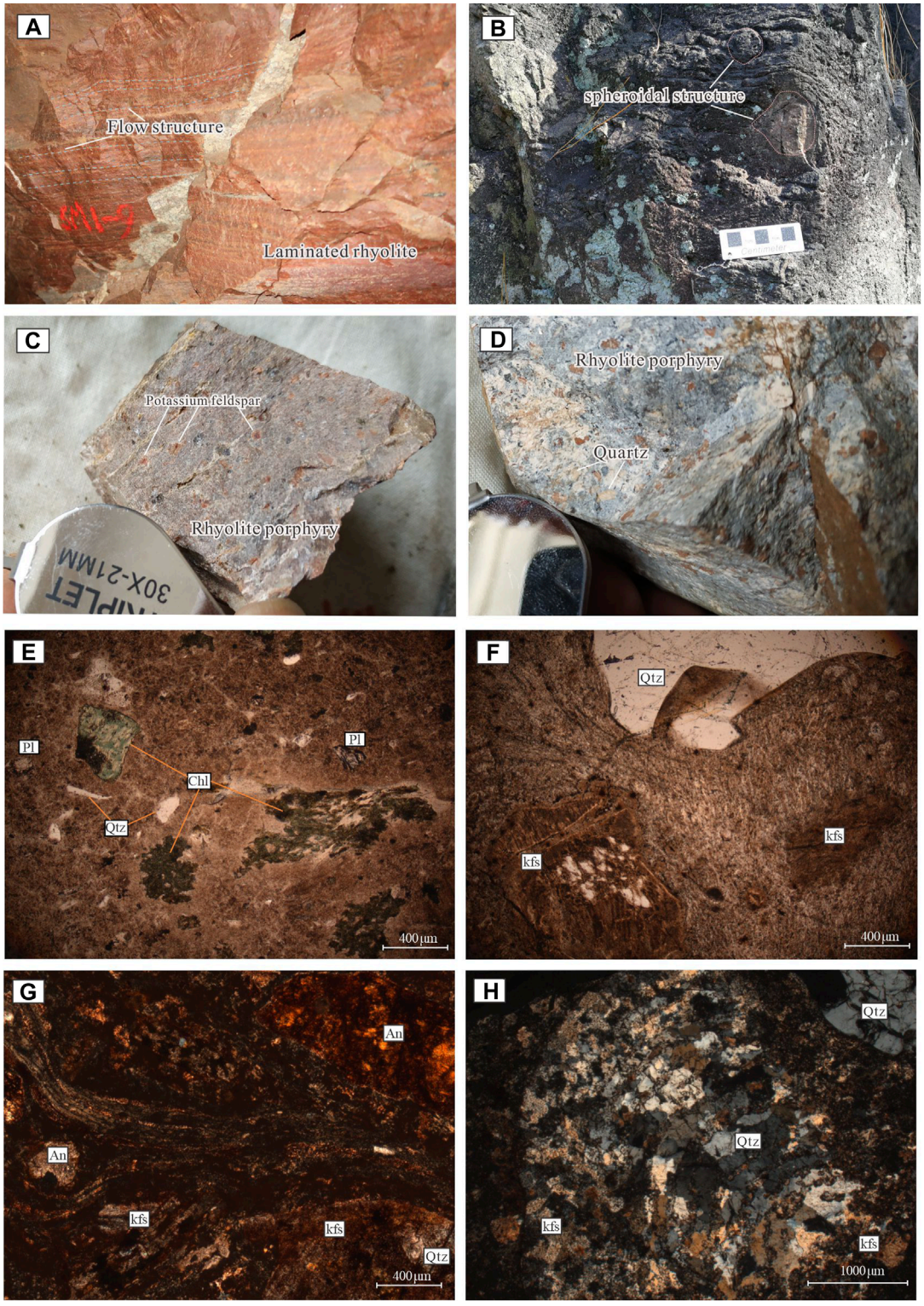

FIGURE 2
Field geology and hand specimens of the rhyolite in the Moganshan Basin **(A)**-Laminated rhyolite; **(B)**- rhyolite and spheroidal structures; **(C, D)**-Rhyolite porphyry is mainly potassium feldspar, sodium feldspar, and quartz grains with a cryptocrystalline matrix; the porphyry has an automorphic-semi- automorphic structureQtz-quartz; Kfs-potassium feldspar; and An-sodium feldspar **(E)**-Rhyolite is porphyritic and rhyolitic. **(F)**-Potassium feldspar porphyry is poorly automorphic, semi-automorphic-automorphic. **(G)**-Sodium feldspar porphyry is even less crystalline, and all are other-shaped. **(H)**-Quartz is mostly dissolved and Portland-like, with rounded sides, semi-automorphic-other-shaped.

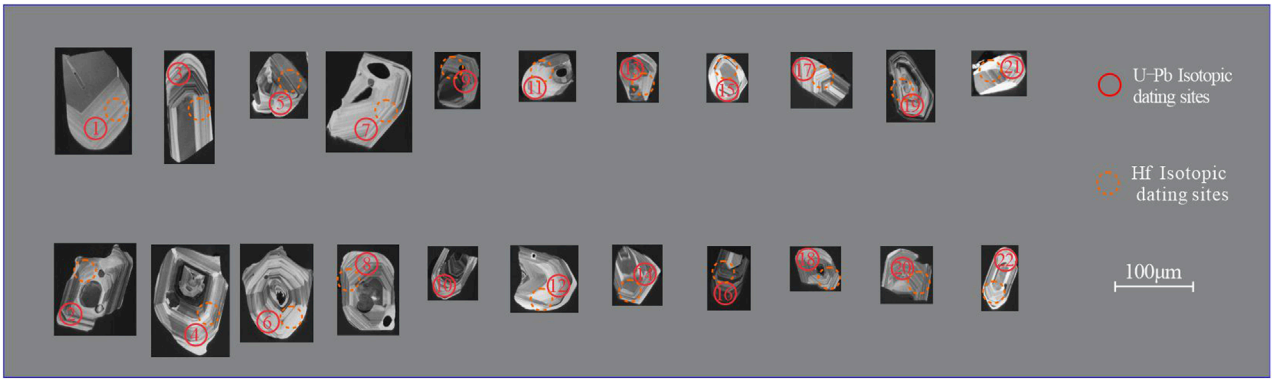

FIGURE 3
Cathodoluminescence photo of rhyolite zircons from the Moganshan Basin.

Cretaceous and Quaternary. The Middle and Lower Silurian are a set of shallow marine siliceous, carbonaceous, muddy and mud-bearing clastic rock strata. The Upper Devonian is a coastal-phase quartz sand conglomerate, and the Upper Carboniferous is a terrace-phase carbonate rock formation; the volcanic activity in the area was stronger during the Mesozoic period, and three phases (andesite, clastic rocks and rhyolitic rocks) characterized by acidic and high alkali were formed within short time intervals. The volcanic stratigraphy is generally unconformable and overlies the Paleozoic strata. The overall direction of fracture development in the area is mainly NE-oriented, followed by NW and NNE-oriented, and these fractures constrain the Mesozoic medium-acidic magmatic intrusion activities in northern Zhejiang (Ma and Xue, 2017; Tang et al., 2018). The regional main fault, the Huzhou-Xuechuan Fault, is 35 km long and 45° in strike, basically controlling the contact boundary between the Late Paleozoic and the Cretaceous (Figure 1B). This fault also controls the Fe-Mo-Au-Sb-B-Pb-Zn mineralization subzone in northern Zhejiang. Volcanic structures are common in the area, and these provide channels for the transport of late mineral-bearing hydrothermal fluids and sites for the precipitation of mineralized materials. The mineral species in the region are relatively rich, with uranium mineral occurrences and large fluorite deposits being the most prominent (Figure 1B).

3 Sample and petrographic characteristics

All the volcanic rock samples were collected from the Moganshan Volcanic Basin, and the lithology is stratified rhyolite and spherical bubble rhyolite (Figure 2). In the hand specimen shown in the figure, the rock is grayish-white and slightly reddish; the mineral crystalline particles are oriented, with flow structure. In addition, the rhyolite porphyry is mainly potassium feldspar, sodium feldspar and quartz particles. The matrix is cryptocrystalline; the size of the porphyry is 0.4–5 mm; and the porphyry is automorphic-semi-automorphic in structure (Figures 2C,D). Microscopically, the rhyolite is porphyritic and rhyolitic in structure (Figures 2E–H); the porphyritic crystals are mainly alkali feldspar (potassium feldspar), sodium feldspar, and quartz; and the matrix is cryptocrystalline. Potassium feldspar porphyry crystals are poorly automorphic, and microscopically visible as residual crystals with quartz account (Figure 2F). The sodium feldspar porphyry crystallization degree is worse; the particle size is 0.1–0.3 mm (Figure 2G). The quartz is mostly dissolved and Portland-shaped, with rounded edges and particle size 1–4 mm; microscopically, small quartz particles can be seen forming stone bubbles (Figure 2H). Serpentinization of the sides of some feldspar grains is also visible under the microscope (Figures 2G,H).

4 LA-ICP-MS zircon U-Pb dating

4.1 Analytical testing

The sample zircon sorting was done at Langfang Geoscience Exploration Technology Co., Ltd., China, and the zircon target making and CL image taking were done at Beijing Gaonianlinghang Technology Co. When testing, to obtain more accurate volcanogenic ages, the zircons with magmatic genesis should be selected as much as possible, as evidenced by clean and transparent crystals, complete crystal structure, no cracks on the crystal surface, no inclusions, and zircon crystals with columnar shape and clear ring-band structure (Wu et al., 2004), in order to obtain more accurate volcanogenic ages (Figure 3). The zircons selected from sample H1931 were pale yellow-colorless and were relatively transparent; they were mainly columnar with semi-automorphic-automorphic crystals, and all zircons were longer than 20 μm. The zircons used for analysis had a clear magmatic rhythmic ring-band structure and light and dark striped structure, features typical of magmatic diagenetic zircons (Hoskin et al., 2000). In this experiment, U-Pb isotope dating was performed on 22 zircons (Table 1), and the measured w (Th) ranged from 37.8×10^{-6} to 374×10^{-6} (mean value 123.28×10^{-6}); w(U) ranged from 55×10^{-6} to 375×10^{-6} (mean value 166.05×10^{-6}); and Th/U values ranged from 0.35 to 1.16, with a mean value of 0.72 (>0.43), The LA-ICP-MS zircon U-Pb dating test analysis was done at the Xi'an Geological Survey Center of the Chinese Geological Survey. Concordia diagrams and weighted mean calculations were constructed using Isoplot 3.0 (Ludwig 2003). The

TABLE 1 LA-ICP-MS zircon U-Pb dating data of the rhyolite in the Moganshan Basin.

Measurement points	$\omega(B)/10^{-6}$		Th/U	$^{207}Pb/^{206}Pb$		$^{207}Pb/^{235}U$		$^{206}Pb/^{238}U$		$^{207}Pb/^{206}Pb$		$^{207}Pb/^{235}U$		$^{206}Pb/^{238}U$	
	Th	U		Ratio	1σ	Ratio	1σ	Ratio	1σ	t/Ma	1σ	t/Ma	1σ	t/Ma	1σ
1	65.8	98.3	0.67	0.0443	0.0070	0.1300	0.0200	0.0209	0.0007	−100	280	123	18	133.3	4.7
2	133.0	169.5	0.78	0.0518	0.0059	0.1480	0.0170	0.0210	0.0007	190	230	139	15	133.8	4.2
3	142.8	210.0	0.68	0.0503	0.0061	0.1330	0.0130	0.0204	0.0009	110	230	126	12	130.1	5.6
4	91.9	143.2	0.64	0.0481	0.0054	0.1330	0.0150	0.0205	0.0009	90	230	129	15	130.9	5.6
5	38.5	67.2	0.57	0.0560	0.0130	0.1540	0.0310	0.0203	0.0013	180	420	141	27	129.5	7.9
6	39.3	65.3	0.60	0.0432	0.0096	0.1200	0.0260	0.0201	0.0012	−240	370	112	24	128.2	7.7
7	88.5	137.2	0.65	0.0510	0.0064	0.1380	0.0180	0.0201	0.0007	130	240	134	17	128.0	4.4
8	146.0	181.0	0.81	0.0517	0.0061	0.1480	0.0170	0.0211	0.0007	220	240	139	15	134.4	4.6
9	139.5	204.4	0.68	0.0516	0.0061	0.1440	0.0160	0.0206	0.0008	160	230	135	14	131.2	4.8
10	37.8	55.0	0.69	0.0500	0.0100	0.1390	0.0290	0.0199	0.0014	80	390	128	26	126.8	8.5
11	46.4	69.7	0.67	0.0522	0.0092	0.1420	0.0230	0.0214	0.0012	120	340	137	23	136.5	7.4
12	158.4	209.6	0.76	0.0448	0.0050	0.1250	0.0130	0.0204	0.0007	−70	220	119	12	130.1	4.4
13	95.2	269.0	0.35	0.0525	0.0054	0.1490	0.0150	0.0209	0.0005	230	210	140	13	133.1	3.3
14	92.0	122.1	0.75	0.0491	0.0077	0.1320	0.0190	0.0202	0.0009	20	300	125	17	128.7	5.6
15	113.3	158.0	0.72	0.0532	0.0066	0.1580	0.0200	0.0217	0.0007	220	240	147	17	138.1	4.3
16	104.3	165.0	0.63	0.0450	0.0051	0.1220	0.0140	0.0198	0.0007	−60	220	116	12	126.3	4.3
17	105.7	196.7	0.54	0.0532	0.0061	0.1420	0.0160	0.0199	0.0007	220	220	134	14	126.7	4.5
18	295.0	310.0	0.95	0.0534	0.0042	0.1510	0.0120	0.0205	0.0006	280	160	142	10	131.1	4.0
19	204.0	176.0	1.16	0.0616	0.0080	0.1790	0.0230	0.0205	0.0007	520	270	165	19	130.6	4.7
20	374.0	375.0	1.00	0.0482	0.0038	0.1360	0.0110	0.0203	0.0005	80	160	129	10	129.4	3.3
21	60.9	92.6	0.66	0.0546	0.0088	0.1480	0.0210	0.0201	0.0012	200	310	138	19	128.0	7.3
22	139.9	178.2	0.79	0.0481	0.0055	0.1300	0.0140	0.0201	0.0007	50	220	127	14	128.2	4.3

10.3389/feart.2024.1399836

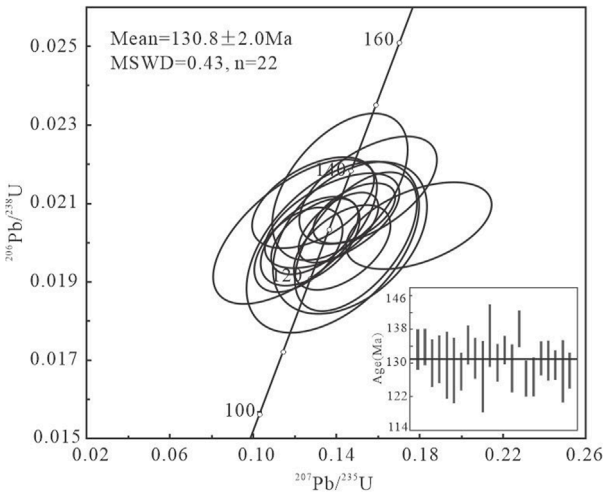

FIGURE 4
U-Pb age harmonization of rhyolite zircon in the Moganshan Basin.

detailed procedure of the experiment can be found in the study of Li et al. (2015).

4.2 Zircon U-Pb ages

The analysis showed that the $^{206}Pb/^{208}U$ age data of these 22 zircons were relatively concentrated, indicating that these age data are largely free of anomalies. In the U-Pb concordance curves of zircons (Figure 4), the measured values of all zircons were located on or near the concordance curves. The weighted average age of $^{206}Pb/^{208}U$ age of these zircons at the 95% confidence level was 130.8 ± 2.0 Ma (mean squared weighted deviation (MSWD) =0.43), which, combined with the characteristics of zircon samples, is considered to represent the age of the bulbous rhyolite in the Moganshan Basin, indicating that this rhyolite is a product of Early Cretaceous volcanism.

5 Geochemical characteristics

5.1 Analytical testing

Based on detailed petrographic observations, the samples were crushed and ground to 200 mesh and sent to Wuhan Sample Solution Analytical Technology Co. The main elements were analyzed with a ZSX Primus II wavelength dispersive X-ray fluorescence spectrometer (XRF) manufactured by Rigaku, Japan, with a relative standard deviation (RSD) of <2%.The detailed analysis procedure is described in GB/T 14506.14–2010 "Chemical analysis of silicate rocks". An inductively coupled plasma mass spectrometer (ICP-MS), Agilent 7700e; Agilent Technologies, United States, was used for the analysis of trace elements and rare earth elements, with relative deviation (RD) < 10% and relative error (RE) < 10%. The detailed analysis process is described in the study of Qu et al. (2004).

5.2 Major element characteristics

(1) Characteristics of principal elements

The loss on ignition (LOI) of the samples can approximate the freshness of the samples (Rollinson, 1993; Zhang et al., 2016). The results of the rock principal element analysis (Table 2) showed that the loss on ignition w(LOI) of the measured samples ranged from 0.41% to 0.99%, with values <1%, and thus samples could be considered fresh (Wang and Chen, 2010). The rhyolite of the Moganshan Basin has a high SiO_2 content, with $w(SiO_2)$ of 72.98%–77.32%, with an average content of 76.08%; a high all-alkaline content, ALK (Na_2O+ K_2O), values of 7.15–9.74, with an average value of 8.70; a rich potassium content, with w (K_2O) of 4.87%–7.06%, with an average content of 5.93%; and K_2O/Na_2O values of 1.41–4.34, with an average value of 2.39; Additionally, the rhyolite is Al-poor, with $w(Al_2O_3)$ of 11.89%–14.44%, with an average content of 12.60%; it is Ca-poor, with w (CaO) of 0.09%–0.80%, with an average content of 0.34%; and it is Mg-poor, with w (MgO) of 0.03%–0.45%, with an average content of 0.14%. The rhyolite has high Si, K-rich, calcium-poor, and magnesium-poor characteristics that are similar to those of A-type rhyolite (Gou et al., 2010; Wu, 2013; Peng, 2015).

The rhyolite of the Moganshan Basin has a high differentiation index (DI) ranging from 90.17 to 97.87 with a mean value of 95.61, and a low consolidation index (SI) ranging from 0.34 to 4.87 with a mean value of 1.45. The rhyolite shows a high degree of magma differentiation, strong segregation and crystallization, and high acidity.

5.3 Trace element characteristics

The results of trace element analysis and corresponding characteristic parameters of rhyolite samples from the Moganshan Basin are shown in Table 3. From the standardized spider web diagram of the original mantle of trace elements (Figure 5A), it can be seen that all rhyolite samples have a consistent distribution form.

The rhyolites are significantly enriched in large ionic lithophilic elements (LILEs) (Rb, Th, U, and K) and relatively enriched in some LREE (La and Ce) elements; they are strongly deficient in high field strength elements (HFSEs) (Nb, Ta, P, and Ti) and LILEs (Ba and Sr), and are relatively deficient in HFSEs (Zr and Hf) and some HREEs. These characteristics of trace elements suggest that the magma may be crustal in origin and are consistent with typical A-type rhyolites (Whalen et al., 1987a; Herget et al., 2007). The rhyolite is strongly deficient in large ionic lithophilic elements Ba and Sr (Ba content ranges from 70.69×10^{-6} to 767.07×10^{-6} with a mean value of 204.25×10^{-6}; Sr content ranges from 17.29×10^{-6} to 132.89×10^{-6} with a mean value of 54.36×10^{-6}). On the Zr-Ba-Sr triangle diagram (Figure 5B), the rhyolite samples generally fall into the low Ba-Sr rhyolite range, indicating that the rhyolite in the Moganshan Basin is a typical low-Ba-Sr rhyolite-like rock (Zhang et al., 2020). This implies crystalline differentiation of alkali feldspar and plagioclase or residual in the source area during magmatic evolution. The rhyolite is strongly deficient in HFSEs (P and Ti) (w (P_2O_5) of 0.01%–0.09%, average 0.03%; w (TiO_2)

10.3389/feart.2024.1399836

TABLE 2 Main element (wt%) characteristics and main rock parameters of the rhyolites in the Moganshan Basin.

Sample number	H1931	H1928	H1929	H1933	H1937	H2109	H2111	H2113	H2114
SiO_2	76.89	76.95	77.32	76.55	75.80	75.43	76.77	72.98	76.07
TiO_2	0.10	0.10	0.09	0.11	0.14	0.12	0.09	0.36	0.10
Al_2O_3	12.48	12.12	11.89	12.08	12.57	13.19	11.90	14.44	12.71
TFe_2O_3	1.18	0.75	1.19	1.33	1.69	1.24	0.93	1.30	0.82
MnO	0.03	0.01	0.05	0.01	0.06	0.02	0.04	0.05	0.01
MgO	0.08	0.07	0.18	0.03	0.45	0.06	0.11	0.15	0.14
CaO	0.38	0.11	0.75	0.10	0.80	0.09	0.38	0.25	0.20
Na_2O	3.18	2.23	2.95	1.95	1.34	3.65	2.70	3.49	3.41
K_2O	5.45	7.06	4.87	6.84	5.81	5.16	6.23	6.24	5.70
P_2O_5	0.02	0.02	0.01	0.02	0.03	0.02	0.02	0.09	0.02
LOI	0.68	0.64	0.99	0.59	1.62	0.58	0.66	0.59	0.41
TOTAL	100.46	100.04	100.31	99.61	100.31	99.54	99.84	99.93	99.58
ALK	8.63	9.29	7.83	8.79	7.15	8.81	8.93	9.74	9.11
A/CNK	1.06	1.05	1.03	1.12	1.26	1.12	1.00	1.11	1.04
A/NK	1.12	1.07	1.17	1.14	1.48	1.14	1.06	1.15	1.08
NK/A	0.89	0.94	0.85	0.88	0.68	0.88	0.94	0.87	0.93
AR	2.96	7.33	2.75	6.19	3.30	3.44	2.57	2.81	3.24
Î	2.20	2.54	1.78	2.30	1.56	2.40	2.36	3.16	2.51
$Mg^{\#}$	0.55	0.90	0.66	0.35	0.75	0.49	0.69	1.00	0.90
Q	36.68	36.90	39.81	39.10	43.87	34.49	36.52	28.45	34.10
Or	32.27	41.96	29.00	40.86	34.81	30.85	37.15	37.16	33.99
An	1.76	0.42	3.66	0.40	3.84	0.35	1.77	0.70	0.91
Ab	26.97	19.01	25.18	16.67	11.49	31.23	23.05	29.75	29.11
Hy	0.42	0.19	0.77	0.29	1.63	0.34	0.44	0.37	0.39
TI	0.20	0.19	0.18	0.20	0.27	0.22	0.18	0.69	0.19
Mt	0.96	0.63	0.94	1.09	1.29	1.01	0.77	0.76	0.67
Ap	0.04	0.04	0.03	0.04	0.07	0.04	0.04	0.20	0.04
DI	95.93	97.87	93.99	96.64	90.17	96.57	96.73	95.37	97.19
SI	0.81	0.66	2.00	0.34	4.87	0.57	1.11	1.31	1.36
R1	2707.00	2686.00	2965.00	2813.00	3234.00	2527.00	2704.00	2148.00	2530.00
R2	290.00	254.00	325.00	252.00	360.00	274.00	282.00	320.00	280.00

TABLE 3 Results of trace element analysis (10−6) and corresponding characteristic parameters of the rhyolites in the Moganshan Basin.

Sample number	H1931	H1928	H1929	H1933	H1937	H2109	H2111	H2113	H2114
Li	7.82	5.05	6.00	4.03	8.13	11.2	7.25	3.02	7.13
Sc	4.28	2.71	4.46	3.12	4.83	3.02	2.61	5.12	2.75
V	2.53	4.15	2.80	2.52	9.72	3.61	2.31	15.2	2.23
Cr	0.63	0.78	0.70	0.79	1.40	0.74	0.90	1.31	0.68
Co	0.31	0.18	0.52	0.20	1.51	0.44	0.24	2.17	0.17
Ni	0.42	0.39	0.44	0.80	1.20	0.50	0.41	1.09	0.32
Cu	1.54	2.27	1.84	2.65	1.18	1.79	2.50	1.74	1.47
Zn	47.51	37.49	51.38	31.52	25.03	46.6	71.5	28.9	19.0
Sr	120.75	40.25	132.89	17.29	124.04	125.7	28.3	118	23.9
Zr	135.64	146.57	127.58	136.93	141.06	155	145	241	145
Sn	3.15	2.85	3.58	3.10	4.28	1.77	2.31	1.62	2.50
Cs	4.42	3.75	3.31	4.62	6.74	2.09	2.87	2.23	3.13
Hf	4.72	5.04	4.80	4.60	5.03	5.57	5.11	6.69	5.32
Ga	17.28	17.62	16.52	16.87	17.51	18.4	16.5	20.0	17.9
Rb	185.45	236.22	172.81	284.24	190.16	179.46	205	184	218
Ba	79.98	88.99	211.91	75.66	364.10	107.11	70.7	767	72.7
Th	24.49	23.70	24.66	23.10	23.50	26.55	23.2	23.5	25.1
U	7.90	19.81	7.14	5.29	6.33	5.05	13.1	5.68	6.01
Nb	22.18	21.19	23.62	21.71	23.18	24.60	16.9	18.9	22.5
Ta	1.81	1.73	1.96	1.71	1.91	2.02	1.65	1.57	1.88
Pb	28.66	30.24	36.17	59.13	11.93	33.9	32.3	19.4	19.5
10^4 Ga/Al	2.62	2.75	2.62	2.64	2.63	2.64	2.62	2.61	2.66
Rb/Sr	11.11	5.87	1.30	16.44	2.98	8.28	7.26	1.56	9.10
Rb/Ba	2.88	2.65	0.82	3.76	0.70	1.68	2.90	0.24	2.99

of 0.09%–0.36%, average 0.14%). This indicate that crystalline differentiation of apatite and plagioclase was present in the source area during magmatic evolution. The content of basal compatible components (Cr, Co, and Ni) is very low (Cr content 0.63×10^{-6} to 1.40×10^{-6} with a mean value of 0.88×10^{-6}; Co content 0.17×10^{-6} to 2.17×10^{-6} with a mean value of 0.64×10^{-6}; Ni content 0.32×10^{-6} to 1.20×10^{-6} with a mean value of 0.62×10^{-6}). Rb/Ba values range from 0.24 to 3.76 with a mean value of 2.07, which is much higher than the ratio of primitive mantle Rb/Ba (0.088), indicating that the rhyolite originated from a highly differentiated evolutionary magma. The 10000 Ga/Al values of the samples (2.61–2.75, mean value 2.65) were all greater than the lower limit of A-type rhyolite (2.6), indicating that the rhyolite has the characteristics of A-type rhyolite.

5.4 Rare earth element characteristics

The results of rare earth element analysis and corresponding characteristic parameters of the rhyolites in the Moganshan Basin are shown in Table 4; rhyolites have high total rare earth elements (excluding Y), ΣREE of 129.84×10^{-6} to 250.54×10^{-6} with an average content of 188.42×10^{-6}. Total light rare earth elements were significantly enriched, with (ΣLREE) of 110.28×10^{-6} to 221.56×10^{-6},

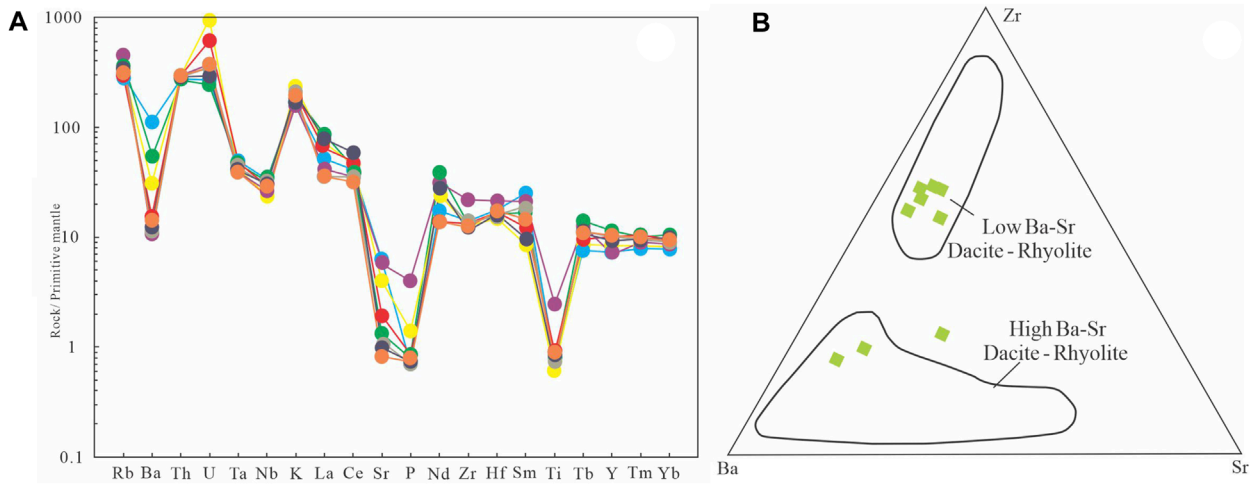

FIGURE 5
Primitive mantle standardized spider web diagram **(A)** and Zr-Ba-Sr diagram **(B)** of trace elements in the rhyolites of the Moganshan Basin.

with an average content of 162.68×10^{-6}. The total amount of heavy rare earth elements (ΣHREE) ranges from 19.56×10^{-6} to 33.00×10^{-6}, with an average content of 25.74×10^{-6} The ratio of light rare earth elements to heavy rare earth elements (ΣL/ΣH) ranged from 5.02 to 7.78, with an average value of 6.29. The $(La/Yb)_N$ values ranged from 4.28 to 8.77, with an average value of 6.25, indicates a clear fractionation between light and heavy rare earth elements. The $(La/Sm)_N$ values ranged from 3.01 to 4.22 with a mean value of 3.58, and the $(Gd/Lu)_N$ values ranged from 0.80 to 1.64 with a mean value of 1.19, indicating a certain degree of fractionation of light rare-earth elements. Compared to light rare-earth elements heavy rare-earth elements fractionation is less pronounced. On the standardized fractionation pattern diagram of rare earth element spheroidal meteorites (Figure 6), all samples had the same pattern of rare earth element fractionation curves, indicating that all rhyolite samples are the products of homogenous magmatic evolution. Because of the enrichment of light rare-earth elements and the fractionation of light and heavy rare-earth elements, the REE fractionation curves showed a right-sloping pattern. In addition, the light rare-earth elements have a certain degree of fractionation, while the heavy rare-earth elements are not clear fractionated. Thus, the REE fractionation curves showed a relatively steep light rare-earth and a gentle heavy rare-earth. The δEu values of rhyolite samples ranged from 0.10 to 0.17, with an average value of 0.15, showing a negative anomaly of europium (Eu). Combined with the characteristics of strong Ba and Sr of trace elements and the distribution pattern being gently concave downward with no pronounced fractionation of heavy rare earth elements, it was found that plagioclase crystallization fractionation or hornblende (instead of garnet) and plagioclase were left in the source during the partial melting process (Huang et al., 2013; Ma and Xue, 2017; Wu et al., 2019; Liu et al., 2020). The δCe values of rhyolites ranged from 0.66 to 1.32, with an average value of 1.06; except for sample H2114 (δCe = 0.66), the δCe values of all samples were close to 1, indicating that the rocks were not affected by low-temperature alteration (Zhou et al., 2000; Liu et al., 2020).

5.5 Sr-Nd-Pb-Hf isotopic signature

(1) Whole-rock Sr-Nd-Pb isotopes

The calculated results for Sr, Nd, and Pb isotopic compositions of the rhyolites from the Moganshan Basin (Table 5) show that these rhyolite samples have relatively consistent initial Sr isotopic values ($(^{87}Sr/^{86}Sr)_i$ and negative ε_{Nd} (t) values, indicating homology among the samples. The $(^{87}Sr/^{86}Sr)_i$ values of the samples ranged from 0.71028 to 0.71160 with a mean value of 0.71094; larger than the mantle magma $(^{87}Sr/^{86}Sr)_i$ values (0.702–0.706) (Faure, et al., 1986). This implies that the magma source was related to crustal materials. The ε_{Nd} (t) values ranged from −6.43 to −5.77, with a mean value of −6.11, and their second-stage Nd isotope pattern age t_{DM2} values ranged from 1,392 to 1,445 Ma, with a mean value of 1,419 Ma. This also suggests that the magma source may be related to immature crustal material (Wu et al., 2017) and may have involved more paleo-medieval crustal material. The $(^{206}Pb/^{204}Pb)_i$, $(^{207}Pb/204\ Pb)_i$, and $(^{208}Pb/^{204}\ Pb)_i$ values of the rhyolite were 18.24–18.76, 15.59–15.62, and 38.22–38.51, respectively; the samples also showed consistent isotopic composition, confirming the homology of the samples.

(2) Zircon Hf isotopes

Based on reliable age, Hf isotope tests of zircons were conducted. The measured points are shown in Figure 3. The results of isotopic compositions of the rhyolites in the Moganshan Basin (Table 6) showed that the Hf isotopic compositions of zircons in rhyolites were relatively homogeneous, with similar ε_{Hf} (t) values and two-stage model ages. The initial Hf isotope values ($^{176}Hf/^{177}Hf$) were 0.282476–0.282596, and the corresponding ε_{Hf} (t) values ranged from −6.43 to −5.77; the two-stage Hf isotopic model age t_{DM2} values ranged from 1,413 to 1,683 Ma, indicating that the material in the magma source area was primarily from the Paleo- and Mesoproterozoic crustal material. On the histogram of zircon ε_{Hf} (t) distribution (Figure 7), the rhyolite exhibited a characteristic single-peaked zircon Hf isotopic composition.

TABLE 4 Results of rare earth element analysis (10−6) and characteristic parameters of the rhyolite in the Moganshan Basin.

Sample number	H1931	H1928	H1929	H1933	H1937	H2109	H2111	H2113	H2114
La	47.12	24.60	34.37	24.44	37.18	28.4	42.7	52.33	57.7
Ce	82.85	60.93	73.43	57.75	73.31	62.9	88.7	104.49	75.2
Pr	10.32	5.23	8.03	5.32	8.63	6.52	9.16	11.67	13.6
Nd	38.12	18.46	30.92	18.83	32.50	23.1	33.2	43.16	52.2
Sm	8.47	4.31	7.36	3.74	7.58	5.41	6.54	9.51	11.1
Eu	0.31	0.21	0.25	0.19	0.42	0.29	0.30	0.40	0.46
Gd	7.09	3.83	6.53	3.88	7.11	5.27	5.94	8.56	9.52
Tb	1.19	0.81	1.15	0.77	1.20	1.02	0.93	1.34	1.50
Dy	7.05	5.21	7.19	5.07	7.74	6.67	5.96	7.80	8.54
Ho	1.50	1.11	1.45	1.15	1.62	1.39	1.17	1.49	1.65
Er	4.50	3.59	4.46	3.53	4.44	4.65	3.92	4.20	5.17
Tm	0.69	0.58	0.71	0.60	0.73	0.74	0.61	0.66	0.75
Yb	4.49	3.85	4.55	3.98	4.68	4.76	4.06	4.28	5.16
Lu	0.68	0.59	0.70	0.59	0.70	0.71	0.60	0.64	0.72
ΣREE	214.39	133.30	181.09	129.84	187.83	151.87	203.67	250.54	243.21
ΣLREE	187.19	113.74	154.36	110.28	159.61	126.66	180.48	221.56	210.22
ΣHREE	27.20	19.57	26.73	19.56	28.22	25.21	23.19	28.98	33.00
ΣL/ΣH	6.88	5.81	5.77	5.64	5.66	5.02	7.78	7.65	6.37
$(La/Yb)_N$	7.53	4.58	5.42	4.41	5.69	4.28	7.53	8.77	8.02
$(La/Sm)_N$	3.59	3.68	3.01	4.22	3.17	3.39	4.21	3.55	3.36
$(Gd/Lu)_N$	1.29	0.80	1.16	0.82	1.25	0.92	1.23	1.64	1.64
δEu	0.12	0.16	0.11	0.15	0.17	0.17	0.15	0.13	0.14
δCe	0.92	1.32	1.08	1.24	1.00	1.13	1.10	1.04	0.66

Note: $\delta Eu = w(Eu)_N/[(w(Sm)_N + w(Gd))]_N^{1/2}$; $\delta Ce = w(Ce)_N/[(w(La)_N + w(Pr)_N)]^{1/2}$; normalized values according to the study of Sun et al.

6 Discussion

6.1 Classification of magma genesis

(1) Rock classification naming

The rock-forming minerals of volcanic rocks are mostly cryptocrystalline, and their compositions are highly variable and not easy to identify. Usually, the all-alkaline-silica (TAS) diagramming method recommended by the International Union of Geological Sciences (IUGS) is used to classify rock types for naming, and some researchers have also used the Zr/TiO_2-Nb/Y diagramming method to name rocks in some special environments (Winchester and Floyd, 1977; Peng, 2015). In this paper, we used the total alkali-silica (TAS) diagram and the Zr/TiO_2-Nb/Y diagram (Winchester and Floyd, 1977), which consists of trace elements such as Nb, Y, Zr, and Ti that are less affected by alteration and metamorphism, and these two diagrammatic methods were used for rock classification discrimination. The rhyolite in the Moganshan Basin is on the TAS diagram (Figure 8A), and all sample points fall within the area of the rhyolite. On the Zr/TiO_2-Nb/Y diagram (Figure 8B), all sample points fall within the rhyolite range except for one sample (that was within the rhyolitic inclusions/inclusion area). The results indicate that the rock type of the collected samples is rhyolite.

On the TAS diagram, nearly all sample points fell in the lower region of the alkaline series. Combined with the rock geochemical

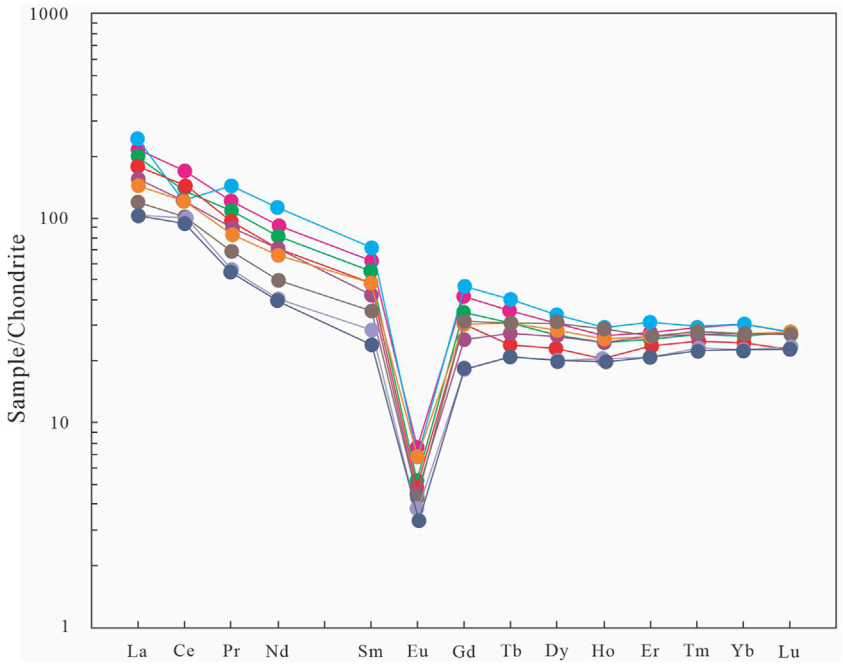

FIGURE 6
Standardized distribution pattern of rare earth element spheroidal meteorites in the rhyolites of the Moganshan Basin (standardized values according to the study of Sun and McDonough, 1989).

parameters (Table 2), such as alkalinity rate (AR), except for two anomalies (6.19, 7.33), the rest of the values were in the range of 2.57–3.44, with a mean value of 3.01. The Rittman index (δ, combination number) was 1.56–3.16, with a mean value of 2.31, and all rock samples had δ values <3.3, indicating that the rhyolite samples were calc-alkaline rocks. The aluminum saturation index (Sander index) (A/CNK) values of the samples ranged from 1.00 to 1.26, with an average value of 1.09; A/NK values ranged from 1.06 to 1.48, with an average value of 1.16. On the A/CNK-A/NK diagram (Figure 8C), all sample points fell in the peraluminous range and were concentrated in the weakly peraluminous range, indicating that the rhyolite is a peraluminous rock. The K_2O/Na_2O values of the samples ranged from 1.41 to 4.34, with an average value of 2.39, showing potassium-rich characteristics. On the Na_2O-K_2O diagram (Figure 8D), five sample points fell in the high-potassium rock series, and four sample points fell in the potassium range; these four sample points were concentrated near the high-potassium-potassium partition line. Therefore, we believe that these samples showed high potassium characteristics overall.

The main-weight element characteristics of the rhyolites in the Moganshan Basin showed that the rhyolites were highly Si-rich, K-rich, and Ca- and Mg-poor, similar to the main-weight element characteristics of the A-type rhyolites. Trace element characteristics showed that the rhyolite was strongly enriched in LILEs (Rb, Th, U, and K) and relatively enriched in some LREE (La and Ce) elements; it was strongly deficient in HFSEs (Nb, Ta, P, and Ti) and LILEs (Ba and Sr), and relatively deficient in HFSEs (Zr and Hf) and some HREEs. The samples' 10000 Ga/Al values (2.61–2.75, mean 2.65) were greater than the lower limit of A-type rhyolites (2.6); the morphology of the trace element primitive mantle standardized spider diagram (Figure 5) was consistent with that of A-type rhyolites. These characteristics of rhyolite trace elements were consistent with those of typical A-type rhyolites (Whalen et al., 1987b; Herget et al., 2007). Meanwhile, the standardized allotment pattern map of rare earth element spheroidal meteorites in the rhyolites of the Moganshan Basin was also consistent with the allotment pattern map characteristics of A-type rhyolites. On the rhyolite10^4 Ga/Al-Zr mapping (Figure 9A), all rhyolite sample points fell within the area of type A magmatic rocks; on the SiO_2-Nb mapping (Figure 9B), all sample points fell within the area of type A magmatic rocks, except one sample point that fell between type I and type A magmatic rocks. From the main, trace, and rare earth element characteristics of the rhyolites and the rhyolite rock type discrimination diagrams, the rhyolites in the Moganshan Basin are type A. After Loiselle and Wones proposed the concept of type A magmatic rocks in 1979, they were defined as alkaline, water-poor, and non-mountain-forming magmatic rocks. In addition, some A-type magmatic rocks were formed in a post-formation environment (Eby, 1990; 1992; Bonin, 2007). On the Y-3Ga-Nb and Y/Nb-Rb/Nb diagrams (Figures 9C,D), the Moganshan Basin A rhyolite types were further discriminated, and all sample points fell within the A2-type (formed in a post-orogenic environment) rhyolite range. In conclusion, the rhyolite of the Moganshan Basin is a peraluminous high-potassium-calcium-alkaline A2-type (formation and post-formation environment) rhyolite.

TABLE 5 Results of Sr-Nd-Pb isotope analysis and related parameters of the rhyolites in the Moganshan Basin.

Sample number	H1937	H1929	H1931	H2109
$^{87}Rb/^{86}Sr$	4.4390	3.7655	4.4472	4.1354
$^{87}Sr/^{86}Sr$	0.718913	0.718560	0.719378	0.717916
2σ	0.000008	0.000009	0.000009	0.000008
$(^{87}Sr/^{86}Sr)_i$	0.71071	0.71160	0.71116	0.71028
$\varepsilon_{Sr}(t)$	90.30	103.00	96.70	84.20
$^{147}Sm/^{144}Nd$	0.1410	0.1440	0.1343	0.1413
$^{143}Nd/^{144}Nd$	0.512275	0.512281	0.512289	0.512261
2σ	0.000006	0.000007	0.000005	0.000006
$(^{143}Nd/^{144}Nd)_i$	0.512155	0.512159	0.512175	0.512141
$\varepsilon_{Nd}(t)$	−6.16	−6.08	−5.77	−6.43
t_{DM1}	1832	1897	1,651	1868
t_{DM2}	1,423	1,417	1,392	1,445
$^{206}Pb/^{204}$ Pb	18.9408	18.8177	18.7848	18.9502
2σ	0.001	0.001	0.001	0.001
$^{207}Pb/^{204}$ Pb	15.6284	15.6291	15.6179	15.6295
2σ	0.001	0.001	0.000	0.001
$^{208}Pb/^{204}$ Pb	39.0627	38.7975	38.8057	38.7981
2σ	0.002	0.002	0.001	0.002
$(^{206}Pb/^{204}$ Pb$)_i$	18.243	18.560	18.468	18.755
$(^{207}Pb/^{204}$ Pb$)_i$	15.594	15.617	15.602	15.620
$(^{208}Pb/^{204}$ Pb$)_i$	38.215	38.506	38.420	38.462

Note: The data were processed using Prof. Yuanfa Lu's Geokit software, and the Sr, Nd, and Pb isotope ratio ages were corrected using zircon U-Pb age of 130 Ma.

6.2 Separation and crystallization

The rhyolite of the Moganshan Basin has a high DI ranging from 90.17 to 97.87, with a mean value of 95.61, and a low consolidation index (SI) ranging from 0.34 to 4.87, with a mean value of 1.45, indicating a high degree of magma differentiation, strong segregation crystallization, and high acidity. On the Yb-Tb/Yb diagram (Figure 10A) and Zr-Th/Nb diagram (Figure 10B), the samples showed consistent characteristics and trends of segregation crystallization, indicating that the magma formed by partial melting of magnesian-iron rocks (intermediate basalt) in the lower crust underwent strong crystallization differentiation during evolution and were finally ejected from the surface to form the Moganshan Basin A-type rhyolite. The absence of magnesian-iron rocks in the basin and the porphyritic structure of the rhyolite suggest that the magma stayed in the shallow magma chamber of the crust before the eruption and had enough time to undergo strong segregation and crystallization.

6.3 Characteristics of the magma source area

The rhyolite samples are significantly enriched in LILEs (Rb, Th, U, and K) and relatively enriched in some LREE (La and Ce) elements. In addition, the samples were strongly deficient in HFSEs (Nb, Ta, P, and Ti) and LILEs (Ba and Sr), and relatively deficient in HFSEs (Zr and Hf) and some HREEs. These characteristics of trace elements suggest that the magma may have originated from the Earth's lower crust. The content of basal compatible components (Cr, Co, and Ni) were very low (Cr content was 0.63 × 10^{-6} to 1.40 × 10^{-6} with a mean value of 0.88 × 10^{-6}; Co content was 0.17 × 10^{-6} to 2.17 × 10^{-6} with a mean value of 0.64 × 10^{-6}; Ni content was 0.32 × 10^{-6} to 1.20 × 10^{-6} with a mean value of 0.62 × 10^{-6}). Additionally, $Mg^{\#}$ values (0.35–1.00, mean value 0.70) were very low, indicating that the magma is of crustal rather than mantle in origin. The Nb/U (1.07–4.87, mean value 3.13) and Ce/Pb (0.98–6.15, mean value 3.10) of rhyolite samples were significantly smaller than those of primitive mantle Nb/U (30) and Ce/Pb (9), and OIB Nb/U (47 ± 10) and Ce/Pb (25 ± 5) that are similar to those of continental crust Nb/U (10) and Ce/Pb (4) (Lei et al., 2021b). In summary, the magma of the rhyolites in the Moganshan Basin originated from partial melting of the lower crust.

Partial melting of different compositions of crust can produce A-type magmatic rocks: metamorphic sedimentary rocks, submerged crustal remnants without water (Collins et al., 1982), newly formed Mg-Fe lower crust (Frost et al., 1999), and longitudinal rocks in the shallow crust (Creaser et al., 1991). On the Nb/Y-Rb/Y diagram of rhyolite (Figure 11), all sample points fell between the upper and lower crust and were closer to the lower crustal part. On the t-$(^{86}Sr/^{87}Sr)_i$ diagram (Figure 12A), all sample points fell between the spheroidal meteorite and crustal evolution. On the t-ε_{Nd} (t) diagram (Figure 12B), the sample points fell between the line of mantle evolution of the spheroidal meteorite and the line of crustal evolution of the South China Paleo-Medieval. On the $(^{206}Pb/^{204}Pb)_i$–$(^{207}Pb/^{204}Pb)_i$ diagram (Figure 12C), all sample points fell within the lower crust, indicating that the magma originated from the lower crust. On the $(^{206}Pb/^{204}Pb)_i$–$(^{208}Pb/^{204}Pb)_i$ diagram (Figure 12D), all sample points fell above the northern hemisphere Pb reference line, reflecting the enrichment of U, Th, and Pb in the source region. On the t-ε_{Hf} (t) plot (Figure 13A), the sample points fell near the lower crust. On the t-$^{176}Hf/^{177}Hf$ plot (Figure 13B), the sample points also fell near the lower crust. In summary, the rhyolite magma in the Moganshan Basin originated from the lower crust. The magma formed by partial melting of the depleted subduction crust had low TiO_2/MgO and SiO_2 values and high CaO and Al_2O_3 values (Creaser et al., 1991; Patin Douce, 1997), while the major element characteristics of the samples showed high SiO_2, low CaO, and depleted Al_2O_3, indicating that the magma did not originate from the depleted subduction crust. In conclusion, the rhyolite of the Moganshan Basin

TABLE 6 Results of Hf isotope analysis of rhyolite zircon in the Moganshan Basin and related parameters.

Measurement points	Age (Ma)	$^{176}Lu/^{177}Hf$	$^{176}Yb/1^{77}Hf$	$^{176}Hf/^{177}Hf$	2σ	$\varepsilon_{Hf}(t)$	t_{DM1} (Ma)	t_{DM2} (Ma)	$f_{Lu/Hf}$
1	130	0.028559	0.000954	0.282547	0.000021	−5.18	996	1,516	−0.97
2		0.045101	0.001434	0.282575	0.000020	−4.22	969	1,455	−0.96
3		0.030586	0.001014	0.282561	0.000025	−4.68	978	1,485	−0.97
4		0.041902	0.001336	0.282578	0.000027	−4.11	962	1,448	−0.96
5		0.040459	0.001309	0.282540	0.000025	−5.46	1,016	1,534	−0.96
6		0.070563	0.002608	0.282596	0.000031	−3.58	969	1,413	−0.92
7		0.065914	0.002488	0.282476	0.000036	−7.83	1,142	1,683	−0.93
8		0.034678	0.001106	0.282564	0.000024	−4.61	977	1,480	−0.97
9		0.041784	0.001383	0.282557	0.000016	−4.86	994	1,497	−0.96
10		0.057500	0.001870	0.282591	0.000018	−3.69	957	1,421	−0.94
11		0.056666	0.001873	0.282530	0.000017	−5.88	1,046	1,560	−0.94
12		0.041309	0.001353	0.282557	0.000015	−4.86	992	1,495	−0.96
13		0.060434	0.001926	0.282532	0.000020	−5.81	1,044	1,555	−0.94
14		0.027625	0.000912	0.282562	0.000022	−4.65	974	1,482	−0.97
15		0.035803	0.001156	0.282561	0.000017	−4.72	982	1,486	−0.97
16		0.032818	0.001072	0.282566	0.000016	−4.5	972	1,473	−0.97
17		0.042868	0.001395	0.282558	0.000015	−4.82	992	1,493	−0.96
18		0.085010	0.002550	0.282544	0.000032	−5.42	1,045	1,532	−0.92
19		0.058798	0.001794	0.282573	0.000019	−4.33	981	1,461	−0.95
20		0.067319	0.002077	0.282574	0.000021	−4.33	987	1,460	−0.94
21		0.059613	0.001999	0.282552	0.000019	−5.07	1,017	1,510	−0.94

Note: The data were processed using Prof. Yuanfa Lu's Geokit software, and the Hf isotope ratio age correction was applied to the zircon U-Pb age of 130 Ma.

10.3389/feart.2024.1399836

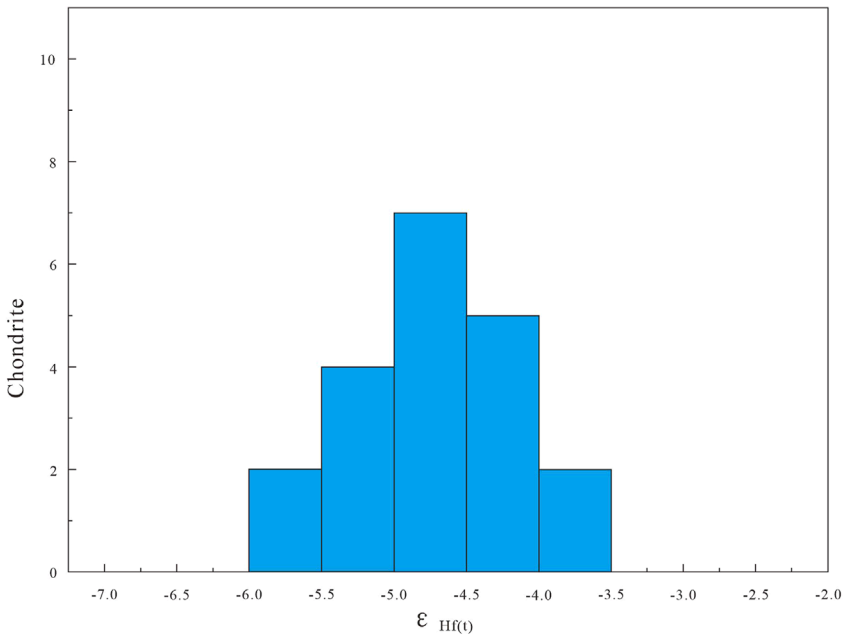

FIGURE 7
Histogram of the distribution of zircon ε_{Hf} (t) in the rhyolites of the Moganshan Basin.

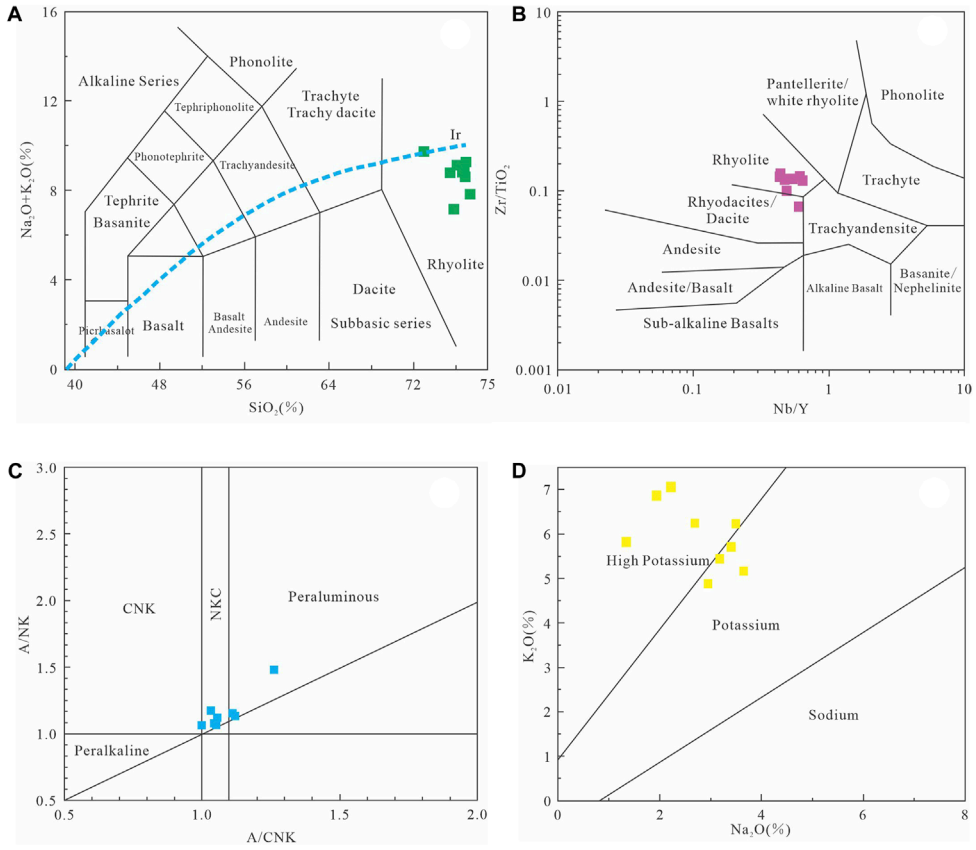

FIGURE 8
TAS illustration and Zr/TiO_2-Nb/Y illustration of the rhyolite in the Moganshan Basin **(A)** TAS illustration (bottom panel according to the study of Le Bas, 1986); **(B)** Zr/TiO_2-Nb/Y illustration (bottom panel according to the study of Winchester and Floyd, 1977); **(C)** A-A/CNK-A/NK diagram (bottom panel according to the study of Richwood et al., 1989); **(D)** B-Na_2 O-K_2 O diagram (bottom panel according to the study of Yip Fat-Wang, 2001).

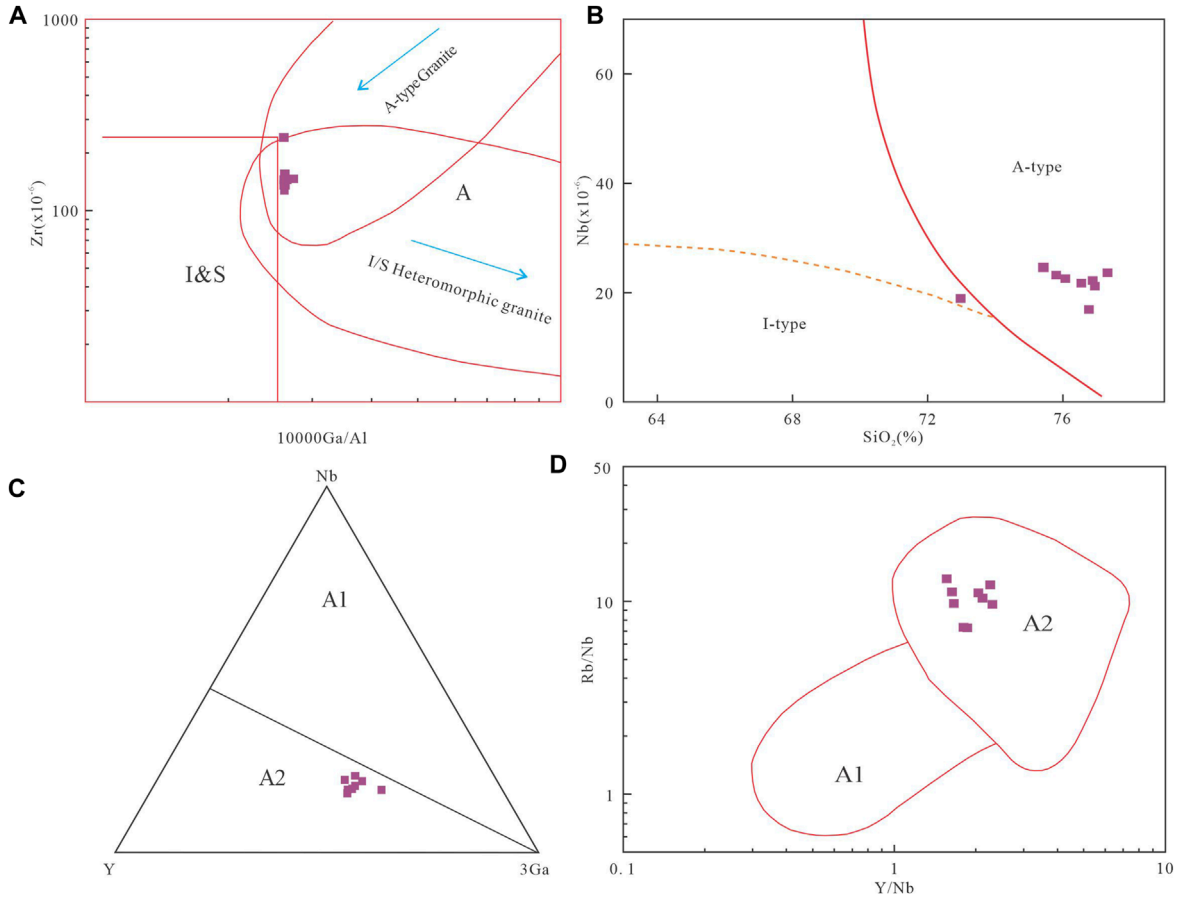

FIGURE 9
Illustration of rhyolite-type discrimination in the Moganshan Basin **(A)** 10^4 Ga/Al-Zr diagram (bottom panel according to the study of Whalen et al., 1987a); **(B)** SiO_2-Nb diagram (bottom panel according to the study of Collins et al., 1982); **(C)** Y-3Ga-Nb diagram (bottom panel according to the study of Eby, 1992); and **(D)** Y/Nb-Rb/Nb diagram (bottom panel according to the study of Eby, 1992)—A1, non-mountain-building environment; A2, post-formation environment.

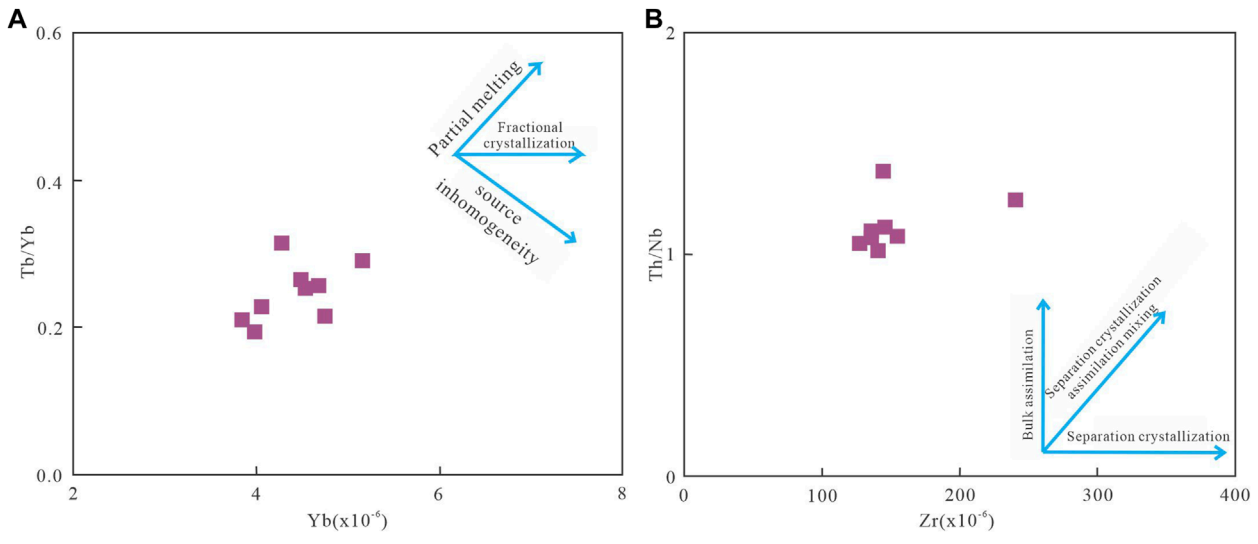

FIGURE 10
Yb-Tb/Yb diagram and Zr-Th/Nb diagram of the rhyolite in the Moganshan Basin **(A)** Yb-Tb/Yb diagram; **(B)** Zr-Th/Nb diagram (bottom panel according to the study of Ma and Xue, 2017).

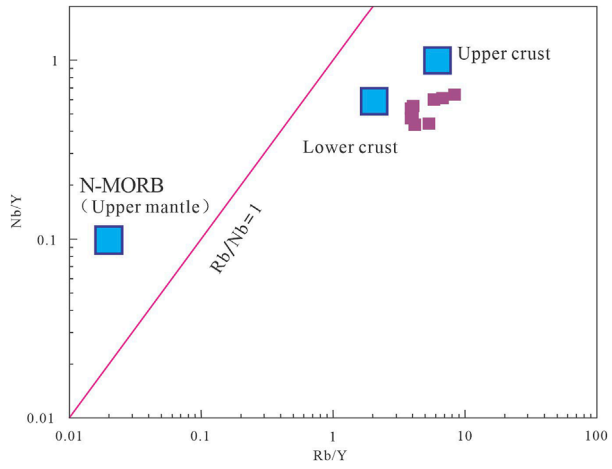

FIGURE 11
Nb/Y-Rb/Y illustration of the rhyolite in the Moganshan Basin (according to the study of Ma and Xue, 2017).

originated from partial melting of the newly formed Mg-Fe subduction crust.

6.4 Rock-forming tectonic environment

The rhyolites of the Moganshan Basin are characterized by high-potassium-calcium alkalinity and are A2-type rhyolites (formed in a post-formation environment); usually, A-type magmatic rocks form in a series of extensional tectonic settings such as post-continental arc extension, post-collisional extension, and intraplate extension (Whalen et al., 1987a; Eby, 1992).

Starting from the Late Mesozoic (approximately 170 Ma), the Kula-Pacific plate interacted with the Asian continental plate, causing the eastern part of China to gradually enter the active continental margin tectonic environment (Ma and Xue, 2017). In the study area, under the post-(collisional) orogenic environment, the demolition and sinking of the lithosphere (or the breakup of the subducting plate) led to a change in the stress state from extension to tension; the rising soft rheospheric material heated the magnesian-iron subcrust by conduction, resulting in partial melting of the magnesian-iron subcrust. In addition, the parent magma (probably andesitic-dacitic) formed and stayed in the shallow upper crust and evolved by separation and crystallization. Finally, the highly differentiated magma was ejected from the surface to form the rhyolites in the Moganshan Basin.

6.5 Uranium mineralization potential

Regionally, the Moganshan Basin is adjacent to the Ganhang volcanic tectonic belt, and uranium mineralization is closely related to the Early Cretaceous volcanism. Additionally, the regional geological evolution of the Xiangshan uranium field in the Ganhang volcanic tectonic belt shows that the tectonic belt experienced regional metamorphism and deformation during the Jinning and Garidonian periods that caused the uranium in the basalt metamorphic rocks of the volcanic basin to precipitate and enrich at favorable levels to form uranium-rich strata (Fan et al., 2003). The Qingbaikouian metamorphic rocks in the basal part of the volcanic basin can provide good conditions for uranium (Zhou 2015; Guo F. S. et al., 2017). At the same time, magmatism in the region can also cause partial melting of early uranium-rich strata, leading to re-enrichment of uranium in magma to form uranium-rich volcanic rocks (Du, 2011). Volcanic-type uranium ores in China are largely distributed in eastern China, and some researchers have statistically summarized the acidic volcanic rocks associated with volcanic-type uranium ores in eastern China and found that most of the volcanic rocks show the characteristics of A-type magmatic rocks. In addition, Baiyanghe, Dazhou, and Hongshanzi volcanic rocks show the characteristics of A1-type magmatic rocks; Xiangshan and Daqiaowu volcanic rocks show the characteristics of A2-type magmatic rocks (Guo J. L. et al, 2017; Liu et al., 2017; Wu et al., 2017; Zhang et al., 2020; Lei et al., 2021a). Concerning the element characteristics, the main elements were negatively correlated with SiO_2, alkali-rich (K_2O+ Na_2O mean value of 8.9%), relatively potassium-rich (K_2 O/Na_2O mean value of 1.89), and weakly peraluminous-strongly peraluminous characteristics (A/CNK mean value of 1.05). The trace element characteristics were enriched in U, Nb, Ta, Th, Zr, F, Li, and Rb and were deficient in Ti, P, and Ba. The trace elements were enriched in U, Nb, Ta, Th, Zr, F, Li, and Rb; deficient in Ti, P, Ba, Sr, La, and Eu; and high in U (mean value 3.94×10^{-6}) and Th (mean value 22.05×10^{-6}). The rhyolite of the Moganshan Basin has similar characteristics and high mineralization element content (U (mean value 8.48×10^{-6}) and Th (mean value 24.20×10^{-6}), indicating that the Moganshan Volcanic Basin has proper geological conditions for uranium mineralization.

7 Conclusion

(1) Zircon U-Pb dating of the rhyolite in the Moganshan Basin shows 130.8 ± 2.0 Ma, indicating that it is a product of Early Cretaceous volcanism.

(2) Whole-rock geochemistry and Sr-Nd-Pb and zircon Hf isotope studies indicate that the rhyolite of the Moganshan Basin is a peraluminous, high-potassium-calcium-alkaline A2-type (formed in a post-formation environment) rhyolite, and the parent magma was formed in a post-active continental margin (collisional) orogenic environment, with partial melting of the magnesian-iron subcrust caused by lithospheric disintegration (or subduction plate breakup). Additionally, the magma stayed in the shallow upper crust during evolution and evolved by segregation and crystallization to form the highly differentiated magma required for rock formation.

(3) The characteristics of the rhyolites in the Moganshan Basin are similar to those of volcanic rocks associated with uranium mineralization in eastern China, showing strong potential for uranium mineralization.

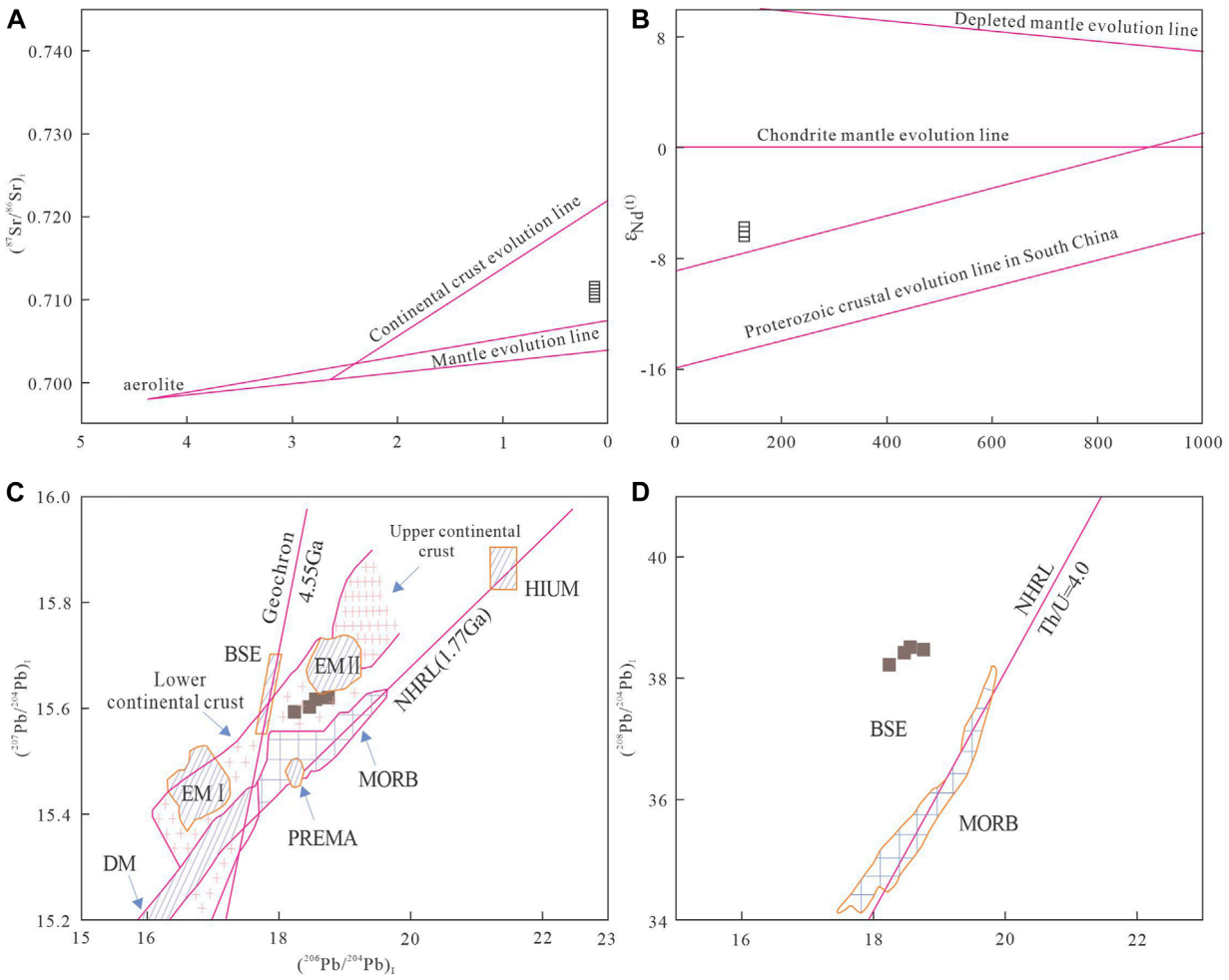

FIGURE 12
Sr-Nd-Pb isotopic composition of the rhyolites in the Moganshan Basin **(A)** t-$(^{86}Sr/^{87}Sr)_i$ illustration (bottom panel according to the study of Rollinson, 1993); **(B)** t-ε_{Nd} (t) illustration (bottom panel according to the study of Shen et al., 1993); **(C)** $(^{206}Pb/^{204}$ Pb)–$(_i^{207}Pb/^{204}$ Pb)$_i$ illustration (bottom panel according to the study of Liu et al., 2020); and **(D)** $(^{206}Pb/^{204}$ Pb)$_i$–$(^{208}Pb/^{204}$ Pb)$_i$ illustration (bottom panel according to the study of Liu et al., 2020).

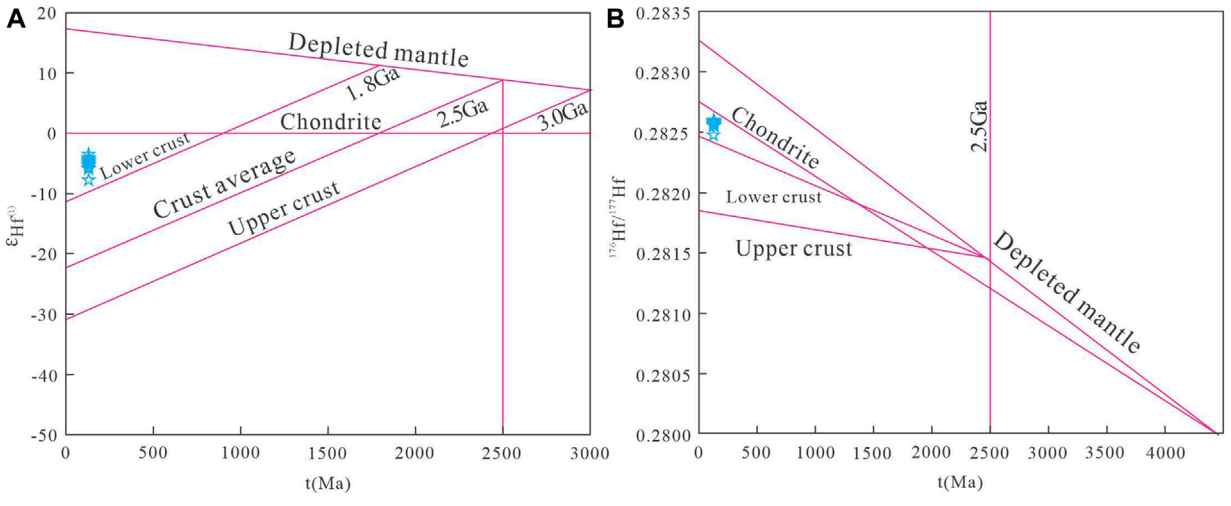

FIGURE 13
Hf isotopic composition of zircon in the rhyolite of the Moganshan Basin **(A)** t-ε_{Hf} (t) graphical solution; **(B)** t-^{176} Hf/^{177} Hf graphical solution (bottom panel according to the study of Zhang et al., 2016).

Data availability statement

The original contributions presented in the study are included in the article/Supplementary material, further inquiries can be directed to the corresponding author.

Author contributions

XW: Writing–review and editing, Writing–original draft. WZ: Conceptualization, Writing–review and editing. SC: Writing–review and editing, Methodology. BW: Writing–review and editing, Methodology. YT: Writing–review and editing, Investigation. WL: Writing–review and editing, Formal Analysis.

Funding

The author(s) declare that financial support was received for the research, authorship, and/or publication of this article. This research was jointly supported by the National Natural Science Foundation of China (Grants: 41902214), the CGS Research Fund (Grants: DZLXJK201904) and the China Geological Survey (Grants: DD20190161, DD20221660-3).

Acknowledgments

We would like to thank No. 262 Geological Party of Zhejiang Nuclear Industry Corp. and State Key Laboratory for Mineral Deposits Research. We also thank Xiaowei Zheng and Huanyuan Chen for his help in the field works.

Conflict of interest

The authors declare that the research was conducted in the absence of any commercial or financial relationships that could be construed as a potential conflict of interest.

Publisher's note

References

Bonin, B. (2007). A-type granites and related rocks: evolution of a concept, problems and prospects. *Lithos* 97 (1-2), 1–29. doi:10.1016/j.lithos.2006.12.007

Collins, W. J., Beams, S. D., White, A. J. R., and Chappell, B. W. (1982). Nature and origin of A-type granites with particular reference to southeastern Australia. *Contributions mineralogy petrology* 80 (2), 189–200. doi:10.1007/bf00374895

Creaser, R. A., Price, R. C., and Wormald, R. J. (1991). A-type granites revisited: assessment of a residual-source model. *Geology* 19 (2), 163–166. doi:10.1130/0091-7613(1991)019<0163:atgrao>2.3.co;2

Dou, X. (2005). REE distribution characteristics of volcanic and epimetamorphic rocks in Xiangshan volcanic basin and discussion on their genesis. *Uranium Geol.* 21 (6), 338–344.

Du, L. T. (2011). On the theory system of hydrothermal uranium metallization in China. *Uranium Geol.* 28. doi:10.1007/s11589-011-0776-4

Duan, Y., Zhao, L. Z., Fan, H. H., and Wang, D. Z. (2001). REE-geochemistry of Mesozoic volcanic-intrusive complex and dark inclusions in Xiangshan district, Jiangxi Province. *Geol. J. China Univ.* 7 (1), 92. doi:10.3969/j.issn.1006-7493.2001.01.011

Eby, G. N. (1990). The A-type granitoids: a review of their occurrence and chemical characteristics and speculations on their petrogenesis. *Lithos* 26 (1-2), 115–134. doi:10.1016/0024-4937(90)90043-z

Eby, G. N. (1992). Chemical subdivision of the A-type granitoids: petrogenetic and tectonic implications. *Geology* 20 (7), 641–644. doi:10.1130/0091-7613(1992)020<0641:csotat>2.3.co;2

Fan, H., Ling, H., Wang, D., Liu, C., Shen, W., and Jiang, Y. (2003). Study on metallogenetic mechanism of Xiangshan uranium ore-field. *Uranium Geol.* 19 (4), 208–213.

Fan, H. H., Lin, H. F., Wang, D. Z., Shen, W. Z., Liu, C. S., and Jiang, Y. H. (2001). Ore-forming material sources for xiangshan uranium 0re-field in jiangxi province: evidence from Nd-Sr-Pb isotopes. *Geol. J. China Univ.* 7 (2), 139.

Frost, C. D., Frost, B. R., Chamberlain, K. R., and Edwards, B. R. (1999). Petrogenesis of the 1.43 Ga Sherman batholith, SE Wyoming, USA: a reduced, rapakivi-type anorogenic granite. *J. petrology* 40 (12), 1771–1802. doi:10.1093/petroj/40.12.1771

Gou, J., Sun, D. Y., Zhao, Z. H., Ren, Y. S., Zhang, X. Y., Fu, C. L., et al. (2010). ZirconLA-CPMS U-Pb dating and petrogenesis of thyolites in Baiyingaolao Formation from the southern Manzhouli/Inner-Mongolia. *Acta Petrol. Sin.* 26 (1), 333–344.

Guo, F. S., Xie, C. F., Jiang, Y. B., Zhou, W. P., Zhang, S. M., Liu, L. Q., et al. (2017a). *Regional geology and uranium polymetallic metallogenic background of xiangshan lugang, jiangxi Province*. Beijing: Geological Publishing House.

Guo, J. L., Jian-Hua, W. U., Guo, H. F., and Wei, C. X. (2017b). Comparison of u-mineralization-related intermediate-acid rocks in eastern China with globlal a-type granite. *Bull. Mineralogy,Petrology Geochem.* 36 (6), 897–904+879.

Han, X. Z., Liu, Q., Hui, X. C., Sun, Z. F., Wang, M. T., Tang, J. W., et al. (2014). Types of uranium and its geological significance in the west segment of Xinlu volcanic basin in Quzhou city,Zhejiang province. *J. Mineralogy Petrology* 34 (4), 15–22.

Hergt, J., Woodhead, J., and Schofield, A. (2007). A-Type magmatism in the western lachlan fold belt? A study of granites and rhyolites from the grampians region, western victoria. *Lithos* 97 (1-2), 122–139. doi:10.1016/j.lithos.2006.12.008

Huang, X. F., Mo, X. X., Yu, X. H., Li, X. W., Ding, Y., Wei, P., et al. (2013). Zircon U-Pb chronology, geochemistry of the Late Triassic acid volcanic rocks in Tanchang area, West Qinling and their geological significance. *Acta Petrol. Sin.* 29 (11), 3968–3980.

King, P. L., White, A. J. R., Chappell, B. W., and Allen, C. M. (1997). Characterization and origin of aluminous A-type granites from the Lachlan Fold Belt, southeastern Australia. *J. petrology* 38 (3), 371–391. doi:10.1093/petroj/38.3.371

Lei, Y., Dai, J., Bai, Q., Wang, K., Sun, L., Liu, X., et al. (2021a). Genesis and implications of peraluminous A-type rhyolite in the haidewula area, east kunlun orogen. *Acta Petrol. Sin.* 37 (7), 1964–1982. doi:10.18654/1000-0569/2021.07.02

Lei, Y., Dai, J., Bai, Q., Wang, K., Sun, L., Liu, X., et al. (2021b). Genesis and implications of peraluminous A-type rhyolite in the haidewula area, east kunlun orogen. *Acta Petrol. Sin.* 37 (7), 1964–1982. doi:10.18654/1000-0569/2021.07.02

Li, B. D. (1993). The origin of porphyroclastic lava and its control over uranium deposits in Xiangshan, Jiangxi: a discussion. *Geol. Rev.* 39 (2), 101–111.

Li, H., Danišík, M., Zhou, Z. K., Jiang, W. C., and Wu, J. H. (2020a). Integrated U–Pb, Lu–Hf and (U–Th)/He analysis of zircon from the Banxi Sb deposit and its implications for the low-temperature mineralization in South China. *Geosci. Front.* 11, 1323–1335. doi:10.1016/j.gsf.2020.01.004

Li, H., Kong, H., Guo, B. Y., Soh Tamehe, L., Zhang, Q., Wu, Q. H., et al. (2020c). Fluid inclusion, H–O–S isotope and rare earth element constraints on the mineralization of the Dong'an Sb deposit, South China. *Ore Geol. Rev.* 126, 103759. doi:10.1016/j.oregeorev.2020.103759

Li, H., Palinkaš, L. A., Evans, N. J., and Watanabe, K. (2020b). Genesis of the Huangshaping W–Mo–Cu–Pb–Zn deposit, South China: role of magmatic water, metasomatized fluids, and basinal brines during intra-continental extension. *Geol. J.* 55, 1409–1430. doi:10.1002/gj.3505

Li, Y. G., Wang, S. S., Liu, M. W., Meng, E., Wei, X. Y., Zhao, H. B., et al. (2015). U-Pb dating study of baddeleyite by LA-ICP-MS: technique and application. *Acta Geol. Sin.* 89 (12), 2400–2418.

Liu, J. G., Li, Z. Y., Huang, Z. Z., Li, X. Z., and Nie, J. T. (2017). The element mobility study of uranium mineralization alteration zones in Xiangshan, Jiangxi using the drill core CUSD3. *Acta Geol. Sin.* 91 (4), 896–912.

Liu, R. R., Li, Z. Y., Tang, J. W., and Xiao-Qi, X. U. (2018a). Study on depth uranium metallogenic model in Dazhou volcanic basin of Zhejiang province. *J. East China Univ. Technol. Sci.* 41 (1), 6–14.

Liu, R. R., Li, Z. Y., Tang, J. W., and Xu, X. Q. (2018b). The source of uranium metallogenic fluid and its migration and enrichment mechanism in Quzhou area, Zhejiang. *J. East China Univ. Technol.* 41 (2), 101–110.

Liu, S., Ma, S. S., Huang, M. H., Wu, J. H., and Guo, H. F. (2020). Geochronology, geochemistry, and geological significance of l-type rhyolite in Nanjing basin, South Jiangxi Province. *Geochimica* 49 (4), 404–421.

Ma, F., and Xue, H. M. (2017). Huzhou-anji Volcanic Basin of northern zejiang province:zircon U-Pb dating, geochemistry and magma genesis. *Acta Geol. Sin.* 91 (2), 334–361.

Pan, C. Y., Wu, Y., Liu, C., Wang, F. G., Tian, J. J., Xu, W., et al. (2021). Genesis of the Dajishan uranium polymetallic deposit in the Xingyi area, Guizhou Province: ore characteristics and occurrence of uranium. *Acta Mineral. Sin.* 41 (1),23–32.

Patino Douce, A. E. (1997). Generation of metaluminous A-type granites by low-pressure melting of calc-alkaline granitoids. *Geology* 25 (8), 743–746. doi:10.1130/0091-7613(1997)025<0743:gomatg>2.3.co;2

Peng, Q. H. (2015). *Geochronological and geochemical characteristics of rhyolite in Xiamajia-Liujiayingzi, Chifeng*. Master Degree Thesis. Nanchang: East China University of Technology. doi:10.16539/j.ddgzyckx.2016.05.011

Rollinson, H. (1993). *Using Geochemical Data: evaluation, presentation, interpretation*. Harlow: British Library Cataloguing-in-Publication Data, 352.

Shao, F., Tang, X., Zou, M., Hu, M., He, X., Chen, X., et al. (2008). Discussion of metallogenic substance source of Xiangshan uranium orefield. *J. East China Geol. Inst.* 31 (1), 39–44.

Sun, S. S., and McDonough, W. F. (1989). Chemical and isotopic systematics of oceanic basalts: implications for mantle composition and processes. *Geol. Soc.* 42 (1), 313–345. doi:10.1144/gsl.sp.1989.042.01.19

Sun, Y., Ma, C., Liu, Y., and She, Z. (2011). Geochronological and geochemical constraints on the petrogenesis of late Triassic aluminous A-type granites in southeast China. *J. Asian Earth Sci.* 42 (6), 1117–1131. doi:10.1016/j.jseaes.2011.06.007

Tang, Z. C., Meng, X. S., Dong, X. F., Wu, X., Chen, Z., Yu, S., et al. (2018). Zircon U-Pb ages and Hf lsotopic compositions of the late mesozoic intrusive rocks in northern Zhejiang: implications for genetic evolution and tectonic environment. *Geotect. Metallogenia* 042 (2), 403–419. doi:10.16539/j.ddgzyckx.2018.02.013

Wang, B., Zhang, W. G., Chen, Z. L., Pan, J. Y., Xu, Z. H., and Liu, X. (2021). A study on ore characteristics and uranium occurrence state of the Zhangjiawu uranium deposit in the northern Zhejiang, China. *Acta Mineral. Sin.* 42 (1), 40–50.

Wang, K. X., Sun, T., Chen, P. R., Ling, H. F., and Xiang, T. F. (2013a). The geochronological and geochemical constraints on the petrogenesis of the Early Mesozoic A-type granite and diabase in northwestern Fujian province. *Lithos* 179, 364–381. doi:10.1016/j.lithos.2013.07.016

Wang, Y., and Chen, S. H. (2010). Element geochemistry and petrogenesis of the volcanic rocks of Zhangjiakou formation in the Zhangjiakou area, North China. *J. Mineralogy Petrology* 30 (1), 75–82. doi:10.1017/S0004972710001772

Wang, Z. Q., Li, Z. Y., and Tang, J. W. (2013b). Deep geodynamic mechanism of the volcanic-type uranium mineralization in Xinlu basin, western Zhejiang province. *Acta Geol. Sin.* 87, 703–714.

Whalen, J. B., Currie, K. L., and Chappell, B. W. (1987a). A-type granites: geochemical characteristics, discrimination and petrogenesis. *Contributions mineralogy petrology* 95 (4), 407–419. doi:10.1007/bf00402202

Whalen, J. B., Currie, K. L., and Chappell, B. W. (1987b). A-type granites: geochemical characteristics, discrimination and petrogenesis. *Contributions mineralogy petrology* 95 (4), 407–419. doi:10.1007/bf00402202

Winchester, J. A., and Floyd, P. A. (1977). Geochemical discrimination of different magma series and their differentiation products using immobile elements. *Chem. Geol.* 20, 325–343. doi:10.1016/0009-2541(77)90057-2

Wu, J. (2013). *Geological age and geochemical characteristics of alkline rhyolites at Hongshanzi basin in South Great Hingan Range*. Master Degree Thesis. Nanchang: East China University of Technology, 1–52.

Wu, J., Song, K., Niu, Z., Guo, H., and Liu, S. (2019). ZirconU-Pb age and geochemical characteristics of the rhyolite of the Yudaokou basin in Weichang, Hebei Province, and their geological implications. *Geol. Bull. China* 38 (7), 1191–1205.

Wu, J. H., Guo, G. L., Guo, J. L., Zhang, Q., Wu, R. G., Yu, D. G., et al. (2017). Spatial-temporal distribution of Mesozoic igneous rock and their relationship with hydrothermal uranium deposits in eastern China. *Acta Petrol. Sin.* 33 (5), 1591–1614.

Wu, Y. B. (2004). Zircon U-Pb ages and oxygen isotope compositions of the Luzhenguan magmatic complex in the Beihuaiyang zone. *Acta Petrol. Sin.* 20, 1007–1024. doi:10.1016/j.sedgeo.2004.06.008

Wu, Y. B., Chen, D. G., Zheng, Y. F., Xia, Q. K., and Tu, X. L. (2004). Trace element geochemistry of zircons in migmatitic gneiss at Manshuihe, North Dabieshan and its geological implications. *Acta Petrol. Sin.* 20 (5), 1141–1150. doi:10.2116/analsci.20.717

Xiao, C. H., Chen, Z. L., Liu, X. C., Wei, C. S., Wu, Y., Tang, Y. W., et al. (2022a). Structural analysis, mineralogy, and cassiterite U–Pb ages of the Wuxu Sb-Zn-polymetallic district, Danchi Fold-and-Thrust belt, South China. *Ore Geol. Rev.* 150, 105150. doi:10.1016/j.oregeorev.2022.105150

Xiao, C. H., Liu, X. H., Yu, P. P., Liu, X. C., Tang, Y. W., Wang, W. L., et al. (2022b). Cassiterite U-Pb dating and micro-XRF analysis constraint on the formation of Xinlu Sn-Zn deposit, South China. *Front. Earth Sci.* 10. doi:10.3389/feart.2022.1031681

Yang, J. H., Wu, F. Y., Chung, S. L., Wilde, S. A., and Chu, M. F. (2006). A hybrid origin for the Qianshan A-type granite, northeast China: geochemical and Sr–Nd–Hf isotopic evidence. *Lithos* 89 (1-2), 89–106. doi:10.1016/j.lithos.2005.10.002

Yang, S., Jiang, S., Jiang, Y., Zhao, K., and Fan, H. (2010). Zircon U-Pb geochronology, Hf isotopic composition and geological implications of the rhyodacite and rhyodacitic porphyry in the Xiangshan uranium ore field, Jiangxi Province, China. *Sci. China Earth Sci.* 53 (10), 1411–1426. doi:10.1007/s11430-010-4058-0

Yang, S. Y., Jiang, S. Y., Zhao, K. D., Jiang, Y. H., and Fan, H. H. (2012). Zircon U-Pb geochronology, geochemistry and Sr-Nd-Hf isotopic compositions of the rhyolite porphyry from the Zhoujiaoshan deposit in Xiangshan uranium ore field, Jiangxi Province, SE China. *Acta Petrol. Sin.* 28 (12), 3915–3928. doi:10.1007/s11783-011-0280-z

Ye, F. W. (2001). *Chronology, Petrology and geochemistry of basic rocks in guangfeng basin, jiangxi Province and their relationship with basin evolution*. China: East China University of Geology, 1–63.

Zhang, L., Li, X., and Wang, G. (2020). The characteristics, research progresses and prospects of volcanogenic uranium deposits. *Acta Petrol. Sin.* 36 (2), 575–588. doi:10.18654/1000-0569/2020.02.15

Zhang, Y. F., Wu, J. H., Jiang, S., Liu, X., Wu, R. G., Liu, S., et al. (2016). SHRIMP U-Pb geochronology, geochemistry and Sr-Nd isotopes of the uranium-(molybdenum) related rhyolite and granitic porphyry, Datan, northern Heibei. *Acta Petrol. Sin.* 32 (1), 193–211.

Zhao, K. D., Jiang, S. Y., Chen, W. F., Chen, P. R., and Ling, H. F. (2013). Zircon U–Pb chronology and elemental and Sr–Nd–Hf isotope geochemistry of two Triassic A-type granites in South China: implication for petrogenesis and Indosinian transtensional tectonism. *Lithos* 160, 292–306. doi:10.1016/j.lithos.2012.11.001

Zou, H., Zindler, A., Xu, X., and Qi, Q. (2000). Major, trace element, and Nd, Sr and Pb isotope studies of Cenozoic basalts in SE China: mantle sources, regional variations, and tectonic significance. *Chem. Geol.* 171 (1-2), 33–47. doi:10.1016/s0009-2541(00)00243-6